Combust. Sci. and Tech., 1998, Vol. 136, pp. 349–371
Reprints available directly from the publisher
Photocopying permitted by license only

Investigation of Reactive Shear Localization in Energetic Solids

R. J. CASPAR, J. M. POWERS* and J. J. MASON

University of Notre Dame, Department of Aerospace and Mechanical Engineering

(Received 7 July 1997; In final form 8 April 1998)

The behavior of an energetic solid subjected to shear is modelled. Data from torsional split-Hopkinson bar (TSHB) experiments are first reduced to calibrate a constitutive model for stress, accounting for the effects of strain and strain rate hardening, in an inert simulant, Mock 900-20, of the high explosive LX-14. This stress model is employed in a transient one dimensional model which includes effects of thermal softening, thermal diffusion, plastic heating, and exothermic reaction. For an event with an average strain rate of $2.8 \times 10^3\,s^{-1}$, reactive shear localization with local strain rates and temperatures in excess of $5 \times 10^4\,s^{-1}$ and 5000 K, respectively, is predicted. It is predicted that within a domain of length comparable to that of the largest heterogeneities, around 250 μm, reaction evolves over sub-nanosecond times scales. Localization and ignition are found to be sensitive to changes in mechanical properties, specific heat, and activation energy, and insensitive to changes in kinetic rate constant, heat release, and thermal conductivity.

Keywords: Shear localization; detonation initiation

1. INTRODUCTION

Initiation of reaction in energetic solids due to mechanical insult is an important, yet poorly understood process. In a typical class of events, a sharp blow will result in an input of mechanical energy into the solid which will initially manifest itself in the form of internally propagating stress waves. These waves will interact with themselves, material interfaces, and boundaries, all the time dissipating mechanical energy into thermal energy. Should the dissipation rate be sufficiently high and concentrated, it may be

*Corresponding author. e-mail: powers@nd.edu

possible to initiate a temperature-sensitive exothermic chemical reaction, which can lead to detonation.

Detonation in solids has been the subject of numerous studies; Fickett and Davis (1979) give a thorough review. There is less understanding of the initiation process induced by mechanical insult, especially for commonly used heterogeneous materials which are insensitive enough to be used in many applications. Many studies, such as that of Baer and Nunziato (1986), use empiricism and modeling assumptions to prescribe when an ignition event has occurred, model the solid as a continuous material beyond its yield stress, and focus on the late-time hydrodynamic events which lead to detonation. There are fewer studies which focus on early time initiation events under dynamic loading conditions in which material strength is important. In this regard, it is thought that the key to initiation is the formation of localized hot spots, *cf.* Field, *et al.* (1982). Mechanisms for hot spot formation are often thought to include jetting, void collapse, viscous heating, shock interaction, friction, and shear localization, also known as shear banding.

We focus on the shear localization mechanism, which is commonly described as follows. A material undergoing a uniform shear stress will in early stages respond by undergoing straining in which the displacement has linear variation with distance. This state is known as homogeneous deformation. Increased straining into the plastic range results in material hardening. In addition, if there is a geometric discontinuity or other material inhomogeneity, straining near that discontinuity will occur at a higher strain rate, which also hardens the material. This increased local deformation also causes plastic heating of the material. If straining occurs at high average strain rates (typically greater than $10^2 s^{-1}$), there is not enough time for generated heat to be conducted away. The local increase in temperature results in thermal softening of the material. If this process dominates over the hardening due to strain and strain rate effects, the material strength decreases. As a result of this local softening, deformation is concentrated into a thin planar region. This final process is known as shear localization or shear banding. Due to the potential concentration of thermal energy in a shear band, it is hypothesized that this energy could trigger a localized reaction in an energetic solid which could spread through the material. In addition, it has been argued by Frey (1981) that this shear banding initiation mechanism is closely related to the friction initiation mechanism in that many of the same ingredients, large localized deformations, viscoplastic work, and large temperature rises, are present in both.

While there is a large body of work describing shear banding (*e.g.*, Bai and Dodd 1992, or Dilellio and Olmstead, 1997) in inert materials, relatively less has appeared for reactive materials. That which exists includes Swallowe and Field (1981); Coffey, *et al.* (1981, 1989); Frey (1981); Field, *et al.* (1985); Kipp (1985); Howe, *et al.* (1985); Dienes (1986); Boyle, *et al.* (1989); Mohan, *et al.* (1989) and Chen *et al.* (1997).

Bai and Dodd review much of the existing experimental evidence supporting shear bands as an ignition mechanism. They conclude that in cyclotetramethylene-tetranitramine (HMX)-based, plastically bonded explosives (PBX), with polyethylene binders that "...it is clear that the susceptibility of some polymers to adiabatic shear banding can have significant effects on the explosiveness of PBXs". Mohan *et al.*, give detailed photographic evidence of shear localization in many reactive materials. Howe *et al.*, show additional photographic evidence of what they call "shear cracks" in TNT subjected to impact loading. These shear cracks are often accompanied by significant material melting and have measured widths of $10-100\,\mu m$. The study of Chen *et al.*, is representative of recent studies of shear localization in various reactive powder metallurgical systems and reports local strain rates up to $10^7\,s^{-1}$ and exothermic reaction initiation.

The theoretical work most relevant to this study is that of Frey, who models a reactive linearly viscoplastic material in which the coefficient of viscosity has temperature dependency. Strain dependency is not included in his constitutive model, nor is his model calibrated to experiments under high strain rate conditions. In some calculations a melt layer is included. The shear band is initiated by assuming that a thin region of width $0.05\,\mu m$ exists which has already shear localized. Also relevant is the study of Dienes, who performs a spatially homogeneous analysis without considering the detailed influence of stress. Lastly, Coffey (1989) gives a complementary discussion and analysis of reactive shear banding on a crystal lattice length scale. Based on an analysis of the motion of dislocations within a crystalline material due to a shock, he estimates shear band widths on the order of $10\,\mu m$; also experimental evidence of shear band formation on nanosecond time scales following shock waves is cited. Coffey rightly suggests that a complete understanding of shear band formation may be impossible in the context of continuum physics and requires consideration of quantum and statistical effects.

While a full theoretical understanding must consider the effects of both material heterogeneities and the finite sized crystal lattice, strong pragmatic reasons remain to render continuum models useful. Practical systems which are currently under widespread examination require consideration of

engineering length scales on the order of up to tens of centimeters, and typical models consider constitutive theories similar to that presented here. A typical two-dimensional calculation of a 20 cm × 20 cm problem on a uniform 2000 × 2000 grid (near the limits of present common computational hardware) fixes a computational cell size at 100 μm, far from molecular length scales, and at scales where modelling of detailed heterogeneity is questionable. Moreover, it is useful to study the properties of continuum models, so as to expose both their inherent abilities and limitations. In fact, once a modeling choice such as that of the existence of a continuum is made, there is an obligation to explore its limiting behavior. One important requirement for continuum models is for solutions to converge as time and space discretization levels approach zero. Another is for those solutions to converge to physically appropriate values. Consideration of such issues for many models of energetic materials, including the present, is always a legitimate exercise, but sometimes leads one into fine scale domains beyond which the models are representative of actual materials. While unsettling, such consideration can have inherent value in provoking either more tempered ambition on the part of modeling efforts or development of accurate subgrid models to better represent the true physics.

This study extends earlier work, especially that of Frey, and is distinguished primarily by the inclusion of an empirically based constitutive model which is believed to be representative of the continuum behavior of the PBX material LX-14, which models the effects of strain, strain rate, and temperature on stress. Additionally, we do not presuppose that shear localization has occurred, but instead allow such a process to develop naturally from a small perturbation. Lastly, we report results which give full details of the temporal development of spatial distributions of velocity, displacement, stress, temperature, and reaction progress; in contrast, earlier results are more limited, which can render assessment more difficult.

The explosive we study, LX-14, is a common PBX material developed at Lawrence Livermore National Laboratory. Dobratz and Crawford (1985) report a chemical formula for LX-14 as $C_{1.52}H_{2.92}N_{2.59}O_{2.66}$. LX-14 is 95.5% mass fraction HMX, a crystalline energetic solid which is formed of particles of diameter of 250 μm or less, bound in a 4.5% mass fraction Estane 5703-P (a co-polymer of polyester and polyurethane) binder. The material, initially in powder form, is pressed to its final form, which at ambient temperature and pressure, is hard and brittle. There is some data for LX-14 which demonstrates the relationship between stress and strain, strain rate, and temperature under quasi-static low strain rate ($\dot{\gamma} < 0.1 s^{-1}$) conditions (*cf.* Groves *et al.*, 1998; Wiegand, 1996). Groves *et al.*, report at

$T = 294\,\text{K}$ and $\dot{\gamma} = 1.25 \times 10^{-5}\text{s}^{-1}$, a peak stress around 10 MPa is reported at a strain of 0.012. The material also exhibited thermal softening; for $T = 333\,\text{K}$, the peak stress decreases to near 3.0 MPa at a strain near 0.01. Some new high strain rate results (Gray *et al.*, 1997) have been obtained for PBX 9501, a very similar material with a slightly different binder. At $\dot{\gamma} = 2000\,\text{s}^{-1}$ a peak stress near 70 MPa is reported, while low strain rate results are similar to that of LX-14.

To outline the paper, we first describe experiments performed to characterize the stress-strain–strain rate behavior. Rather than implementing the resulting constitutive equation into a large scale design code, it can be beneficial to test first in a simpler model. With such a model one can quickly and unambiguously focus on the performance of the constitutive equation in a computational environment which contains the key modeling ingredients: sensitivity of stress to strain, strain rate, and temperature, finite rate exothermic temperature-sensitive chemical kinetics, and thermal diffusion. Such a model is presented. Finally, the sensitivity of the elapsed time to the onset of localization is determined as a function of key mechanical and thermochemical parameters. While we employ a continuum model for the heterogeneous material LX-14 which has particle sizes less than 250 μm, it is noted that the method has sufficient generality to make it well suited to model crystalline reactive materials, for which the heterogeneities typically occur on length scales orders of 0.001 μm (Eiland and Pepinski, 1955).

2. EXPERIMENTAL CALIBRATION TECHNIQUE

A torsional split Hopkinson bar (TSHB) is used to investigate constitutive behavior for material subjected to simple, dynamic shear. The split Hopkinson bar was first adapted for tests in torsion by Baker and Yew (1966); the TSHB as used in this study is discussed by Hartley *et al.* (1985). There are several reasons why the TSHB is appropriate. It can be designed to produce a torsional pulse of almost any length, and hence, large deformation in the specimen is possible. The apparatus can be designed to produce more deformation than the specimen can withstand. In addition, shear is one main form of deformation present in high rate deformation events such as penetration; hence, it is desired to determine behavior in shear, as opposed to compression or tension. Disadvantages of split Hopkinson bar compressive testing result from the Poisson's ratio effect, which gives rise to friction between the specimen and bar. In torsional tests,

there is no Poisson's ratio effect, no radial contraction or expansion and no frictional effects.

There are, however, some limitations to the TSHB. First, tests may only be run on a limited range of average strain rates ($10^2 < \bar{\dot{\gamma}} < 10^4\,s^{-1}$). We note that the overbar indicates a spatial average over the length L of the specimen. In the lower limit, the signal to noise ratio is too low; in the upper limit, the elastic limit of cylindrical bars in the TSHB, described in the following paragraph, is approached. In addition, data analysis for this apparatus assumes homogeneous deformation. Hartley *et al.* (1985) have shown that it takes a few reflections of the loading pulse from the ends of the specimen before a state of homogeneous deformation is reached, thus rendering the early time results of the TSHB inaccurate.

The TSHB, depicted in Figure 1a, consists of two elastic cylindrical bars: an incident and transmission bar, each of length about 3 m; a torsional pulley; and a hydraulic clamp. The two bars are aligned along a common axis, with a thin walled cylindrical specimen joining them. The end of each bar in contact with the specimen is milled to produce a hexagonal socket, into which the specimen or an adaptor is inserted. The adaptor is used for cases in which it is desirable to glue a weak specimen, such as for the material examined in this study, in place, rather than grip it with the hexagonal socket. The torsional pulley is attached to the end of the incident bar far from the specimen, and the clamp is placed at a variable distance from the pulley, typically about 1 m. The clamp is used to prevent rotation of the incident bar while the torsional pulley is rotated, thus storing a torsional pulse in the bar between the pulley and clamp. The sudden release of the clamp propagates an incident shear strain pulse down the incident bar. This pulse reaches the specimen, transmitting some shear strain through the specimen into the transmission bar and reflecting some back into the incident bar. Dimensions of the specimen are given in Figure 1b.

The key to achieving constant strain rate tests is rapid release of the clamp. The clamp is engaged by a hydraulic pump, then hydraulic pressure is increased until a break element fractures, causing the rapid release of the clamp faces. Ideally, the incident pulse would be a square pulse of torsion, with nearly instantaneous rise and fall time and constant magnitude, thus producing deformation in the specimen at a constant strain rate. The typical rise time from 10% to 90% of the maximum strain achieved is 30–50 μs for all tests.

Values of average shear stress, average shear strain and average shear strain rate in the specimen are determined from a standard analysis (Hartley *et al.*, 1985) of the transmitted and reflected strain, γ_T and γ_R, respectively,

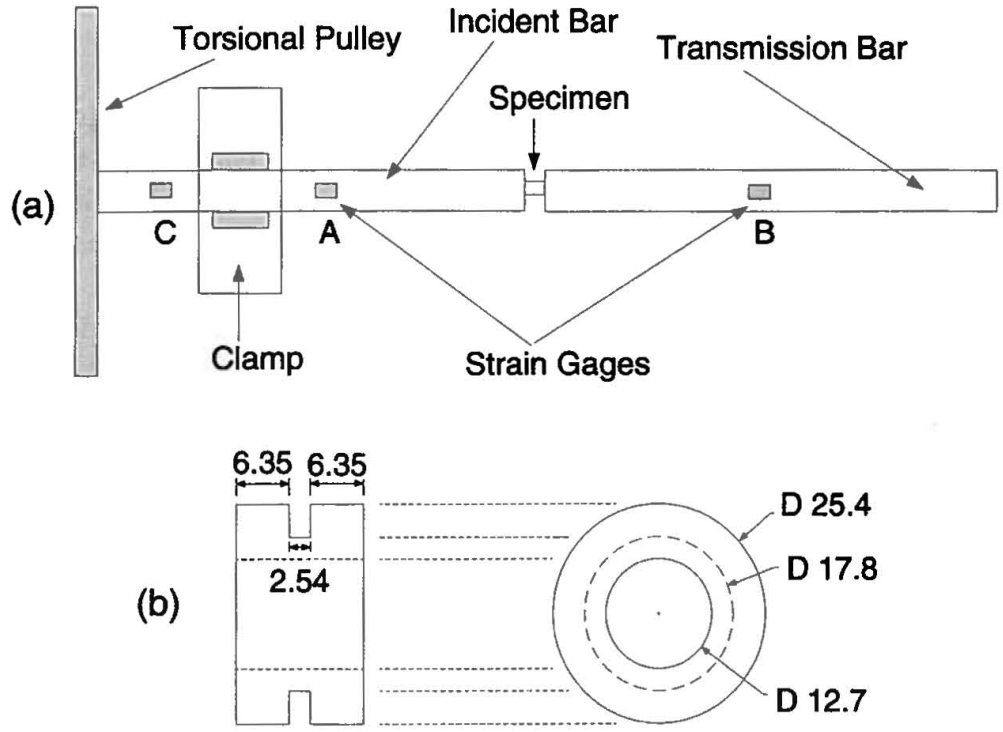

FIGURE 1 (a) Schematic of the TSHB (not to scale); (b) Scaled diagram of the cylindrical specimen used in the TSHB tests (all dimensions in millimeters).

in the transmitting and incident bars:

$$\bar{\tau}(t) = \frac{GD}{8w}\left(\frac{D}{d}\right)^3 \gamma_T(t), \tag{1}$$

$$\bar{\gamma}(t) = -\frac{2\tilde{c}}{L}\left(\frac{d}{D}\right)\int_0^t \gamma_R(\tilde{t})d\tilde{t}. \tag{2}$$

Here $\tilde{c}$ is the elastic shear wave speed in the bar, d is the specimen outer diameter, D is the bar diameter, t is the time, G is the shear modulus of the bar, w is the wall thickness of the specimen, and $\tilde{t}$ is a dummy variable of integration. Strain rate can be determined from differentiation of strain.

Shear strain due to pulses in the both bars are recorded by electric resistance strain gages and Wheatstone bridges. Since the gages are equidistant from the specimen, it is ensured that the reflected and transmitted pulse will arrive at the gages at approximately the same time. There is also a strain gage mounted to record the stored torque, which is used to obtain the expected average strain rate in the specimen.

3. MODEL EQUATIONS

A simple mathematical model with a minimum number of ingredients sufficient to describe shear localization is given here. This model neglects many features of real systems, for example, detailed chemical kinetics, variable material properties, porosity, material compressibility, glass transition, material melting, effects of microstructural heterogeneities, crystal lattice effects, and gas phase behavior of reaction products, which in principle can influence the process, but which are not fundamentally necessary features for localization.

We model a thin walled cylindrical specimen and take z to be the axial distance, θ the azimuthal angle, and r the radial distance. The specimen has a prescribed initial distribution of circumferential velocity, v_θ such that it varies linearly from $v_\theta = 0$ at $z = 0$ to $v_\theta = v_1$ at $z = L$. The following assumptions are made. There is no component of velocity or displacement u in the radial or axial directions: $v_r = v_z = u_r = u_z = 0$. Due to axisymmetric and thin walled geometry, there is no variation in the circumferential or radial direction: $\partial/\partial\theta = \partial/\partial r = 0$. In order to induce localization, we allow the specimen wall thickness to vary with axial position z. We make the *ad hoc* assumption that this perturbation is sufficiently small so as not to introduce gradients in the radial or circumferential directions. Under these assumptions, the stress tensor reduces to one component, $\sigma_{z\theta}$, the stress on the axial face in the circumferential direction, which will be referred to as the shear stress, τ. The work of plastic deformation is assumed to be completely converted to heat. The material is taken to undergo a one-step chemical reaction dictated by Arrhenius kinetics. Density, ρ, thermal conductivity, k, and specific heat c are assumed to be equal in the unreacted and reacted material, and constant. Under these assumptions, the dimensional governing equations are

$$\rho w \frac{\partial v_\theta}{\partial t} = \frac{\partial}{\partial z}(w\tau), \tag{3}$$

$$\rho w \frac{\partial e}{\partial t} = w\tau \frac{\partial v_\theta}{\partial z} - \frac{\partial}{\partial z}(w\tilde{q}_z), \tag{4}$$

$$\frac{\partial u_\theta}{\partial z} = \gamma, \tag{5}$$

$$\frac{\partial u_\theta}{\partial t} = v_\theta, \tag{6}$$

$$\frac{\partial \lambda}{\partial t} = Z(1-\lambda)\exp\left(-\frac{E}{RT}\right), \tag{7}$$

where e is the internal energy per unit mass, $\tilde{q}_z$ is the heat flux in the axial direction, γ is the shear strain, λ is the reaction progress variable, restricted so that $0 \leq \lambda \leq 1$, and T is the temperature. The parameters Z, E, and R are, respectively, the kinetic rate constant, activation energy, and universal gas constant. Equation (3) models conservation of linear momentum. Equation (4) models conservation of energy. Equation (5) is the definition of strain. Equation (6) defines velocity as the time derivative of displacement. Finally, Eq. (7) is a one-step Arrhenius kinetics law. This model predicts a continuous spatial distribution of stress τ and strain γ. Spatial averages of these quantities are employed for later comparison with observations.

The constitutive equations are:

$$\tau = \alpha\left(\frac{T}{T_o}\right)^{\nu}\gamma^{\eta}\left(\frac{\partial\gamma}{\partial t}\frac{L}{v_1}\right)^{\mu}, \tag{8}$$

$$\tilde{q}_z = -k\frac{\partial T}{\partial z}, \tag{9}$$

$$e = cT - \lambda q. \tag{10}$$

Equation (8) is a constitutive law for stress, proposed by Clifton *et al.* (1984) where ν, η, and μ are the exponents which characterize thermal softening, strain and strain rate hardening, respectively, α is a constant with units of stress, and T_o is the ambient temperature. It is noted that while models such as that of Eq. (8) are common in the literature, work remains to be done in demonstrating that multidimensional tensorial extensions can be developed which satisfy the principles of frame and material indifference, along with the entropy inequality. Further, while the constitutive model is likely to behave well within the domain in which it is calibrated, it is not likely to be valid in either the elastic limit or in the fluid limit. Equation (9) is Fourier's law of heat conduction. Equation (10) is a caloric state equation which accounts for energy changes due to chemical reaction.

The following boundary conditions are used:

$$v_\theta(t,0)=0, \quad v_\theta(t,L)=v_1, \quad u_\theta(t,0)=0,$$
$$u_\theta(t,L)=v_1 t, \quad \frac{\partial T}{\partial z}(t,0)=0, \quad \frac{\partial T}{\partial z}(t,L)=0. \tag{11}$$

The velocity and displacement are constructed so that one end is held fixed and the other has a constant velocity. The boundary conditions on temperature are such that the ends of the specimen are insulated. The initial conditions are

$$v_\theta(0,z)=v_1\frac{z}{L}, \quad u_\theta(0,z)=0, \quad T(0,z)=T_o, \quad \lambda(0,z)=0. \tag{12}$$

The velocity distribution is initially linear, and the specimen is initially undisplaced, unreacted and at a uniform temperature. In order to induce localization at the center, the thickness of the tube is perturbed so that it is thinner there. The form of this perturbation is taken to be

$$w=w_0-\frac{h_p}{2}\left[1-\cos\left(\frac{2\pi z}{L}\right)\right]. \tag{13}$$

Here, h_p is the amplitude of the perturbation; the ratio h_p/w_o is maintained at 0.1 in all calculations.

We also introduce a supplementary criterion to quantify commencement of localization. Zener and Hollomon (1944) stated that adiabatic shear bands typically initiate at a point, z, after a maximum stress is reached in the shear stress–shear strain relationship for the material at that point, $(\partial\tau/\partial\gamma)|_z \leq 0$. Adapting this notion for a material for which $\tau=\tau(T,\gamma,\dot\gamma)$ where $\dot\gamma=(\partial\gamma/\partial t)\big|_z$, one can show by application of the chain rule that localization occurs when

$$\left.\frac{\partial\tau}{\partial\gamma}\right|_{T,\dot\gamma}+\left.\frac{\partial\tau}{\partial\dot\gamma}\right|_{T,\gamma}\frac{\partial\dot\gamma/\partial t|_z}{\partial\gamma/\partial t|_z}\leq-\frac{\partial T/\partial t|_z}{\partial\gamma/\partial t|_z}\left.\frac{\partial\tau}{\partial T}\right|_{\gamma,\dot\gamma} \tag{14}$$

The first term represents strain hardening of the material. The second term represents the product of strain rate hardening and a problem-specific factor which is the ratio of the rate of change of strain rate to the rate of change of strain. The right side represents the product of the ratio of the rate of change of temperature to the rate of change of strain and thermal softening. Terms on the left side of Eq. (14) are defined as Ψ and those on the right side as Φ so that the Eq. (14) is expressed as $\Psi\leq\Phi$. By identifying the time when

equality, $\Psi = \Phi$, is achieved, one quantifies the time of onset of shear localization provided the strain and strain rate are monotonically increasing functions in time.

The governing equations are reduced to a form suitable for numerical solution as follows. First, by differentiating Eq. (5) with respect to time and Eq. (6) with respect to space, and equating the results, one determines that $\partial\gamma/\partial t = \partial v_\theta/\partial z$. The relation and Eqs. (5) and (8) are inserted into the linear momentum equation, Eq. (3). The energy equation, Eq. (4), is reduced by similar substitution. Finally, Eqs. (3), (4), (6) and (7) are restated as a system of four non-linear partial differential equations in the four unknowns, v_θ, T, u_θ, and λ:

$$\frac{\partial v_\theta}{\partial t} = \frac{1}{\rho w}\frac{\partial}{\partial z}\left[w\alpha\left(\frac{T}{T_o}\right)^{\nu}\left(\frac{\partial u_\theta}{\partial z}\right)^{\eta}\left(\frac{\partial v_\theta}{\partial z}\frac{L}{v_1}\right)^{\mu}\right], \tag{15}$$

$$\begin{aligned}\frac{\partial T}{\partial t} = \frac{1}{\rho c}\Bigg[&\alpha\left(\frac{T}{T_o}\right)^{\nu}\left(\frac{\partial u_\theta}{\partial z}\right)^{\eta}\left(\frac{\partial v_\theta}{\partial z}\right)^{\mu+1}\left(\frac{L}{v_1}\right)^{\mu} \\ &+ \frac{k}{w}\frac{\partial}{\partial z}\left(w\frac{\partial T}{\partial z}\right) + Z\rho q(1-\lambda)\exp\left(-\frac{E}{RT}\right)\Bigg]\end{aligned} \tag{16}$$

$$\frac{\partial u_\theta}{\partial t} = v_\theta, \tag{17}$$

$$\frac{\partial \lambda}{\partial t} = Z(1-\lambda)\exp\left(-\frac{E}{RT}\right). \tag{18}$$

Using the method described by Whitham (1974), it has been rigorously shown by Caspar (1996) that this system, when linearized about a reference strain rate, is fully parabolic, as all eigenvalues of the resulting characteristic determinant are formally zero. Caspar's analysis can be trivially extended to yield the same conclusions for the full system. Thus, the system can be solved *via* a marching technique; here, a method of lines is used. First, all terms involving spatial derivatives are replaced by a spatial discretization using second order central differences. The result is a set of stiff first order non-linear ordinary differential equations in time. These equations are represented in a Fortran 77 computer code and are numerically solved as an initial value problem with the implicit method embodied in the code LSODE (Hindmarsh, 1983). In all simulations reported here, a domain length of

2500 μm is used, which is broken into 50 finite difference cells, yielding a cell size of 50 μm (somewhat less than the mean size of large particles). In contrast to explicit methods, there is typically no time step restriction for numerical stability for the implicit method. However, a Newton's method iteration is required at each time step to solve a resulting set of non-linear algebraic equations. In order to insure that the implicit solver is able to converge to a solution at each time step, an adaptive time step routine is employed to inhibit large changes in the magnitudes of primitive variables. In the vicinity of localization and reaction events, this imposes severe restrictions on the time step, which often reduces to values less than 10^{-15} s. During periods of such rapid change, a fast time scale is employed numerically to avoid problems associated with finite machine precision. To avoid impractically large data files, we do not plot full details of the time variation, but only values at selected representative points. Nevertheless, results shown are the fruits of a calculation which has a temporal accuracy fully appropriate for the level of spatial discretization employed. Calculations are performed on a Sparc Ultral workstation; a typical case requires about five minutes; although at the halt of calculation, the computational behavior is extremely sluggish due to stiffness. Increases in spatial resolution do not fundamentally alter the results. Additionally, Caspar (1996) described three code verification tests. In each test, exact solutions with time and space variation displayed excellent agreement with numerical simulations. More importantly, the L_2 norm of the global difference between numerical and exact solutions was converging to zero as spatial resolution increased at a rate consistent with second order spatial discretization.

4. RESULTS

This section will present experimental results which we use to form estimates of mechanical properties of LX-14 and theoretical predictions for its behavior in a reactive shear banding situation. For reasons of safety, all tests were performed on an inert simulant known as Mock 900–20. In it, the reactive HMX crystals are replaced with granular barium nitrate and pentek with similar mechanical properties and size distributions. A nearly identical binder is used as for LX-14. The mass fractions are 0.440/0.504/0.042/0.014 barium nitrate/pentek/Estane/tris-beta chloroethylphosphate (CEF). The material was prepared in powder form at Los Alamos National Laboratory as Blend #92–01 and was pressed at Eglin AFB at 20000 psi without heat or vacuum to a density of 1855 kg/m^3.

The parameters employed for what we refer to as the baseline case, are as follows: $\alpha = 42.39 \times 10^6\,\mathrm{N/m^2}$, $\nu = -1.280$, $\eta = 0.320$, $\mu = 0.080$, $\rho = 1849\,\mathrm{kg/m^3}$, $c = 1130\,\mathrm{J/kg/K}$, $k = 0.439\,\mathrm{W/m/K}$, $Z = 5.00 \times 10^{19}\,\mathrm{1/s}$, $q = 5.95 \times 10^6\,\mathrm{J/kg}$, $E = 2.206 \times 10^5\,\mathrm{J/mole}$, $R = 8.314\,\mathrm{J/mole/K}$, $v_1 = 7.00\,\mathrm{m/s}$, $L = 0.0025\,\mathrm{m}$, $w_o = 0.0025\,\mathrm{m}$, $h_p = 0.00025\,\mathrm{m}$, $T_o = 298\,\mathrm{K}$. The parameters ρ, q and k are taken from Dobratz and Crawford (1985) for LX-14. As Dobratz and Crawford do not report a single numerical value for c, but instead give a graphical data showing its weak temperature dependency, we use the reported value for the very similar PBX 9501, which is well within the range reported graphically for LX-14. In order to model thermal softening for some of the materials they tested, Johnson and Cook (1983) assumed a linear decrease in the stress as a function of temperature, with the stress reaching zero at the melting point. Since LX-14 reacts near the HMX melting point, its thermal softening parameter, ν, is chosen such that stress is decreased by approximately 50% at the HMX reaction initiation temperature, 531 K. The remaining mechanical parameters, α, η and μ, are determined from experimental results on explosive simulants. Since LX-14 is overwhelmingly composed of HMX, the values of Z and E for HMX are used. The remaining parameters are chosen to match experimental conditions employed in our specific tests, with the exception that a low strain rate calibration required $v_1 = 0.75\,\mathrm{m/s}$. The baseline case corresponds to an average strain rate of $\bar{\dot{\gamma}} = 2800\,\mathrm{s^{-1}}$, while the low strain rate case has $\bar{\dot{\gamma}} = 300\,\mathrm{s^{-1}}$.

4.1. Constitutive Model Calibration

Figure 2 shows results from tests performed with the TSHB on the LX-14 inert simulant at two different average strain rates along with predictions of this model, each at $T = 298\,\mathrm{K}$. The results are repeatable. The values chosen for α, μ and η result in a reasonably accurate representation of the magnitude and large scale trends observed in the experiments.

The test at the lower average shear strain rate of $\bar{\dot{\gamma}} = 300\,\mathrm{s^{-1}}$ lasted for about 350 μs. The material in this test exhibits an early time stress overshoot, occurring at $\bar{\gamma} = 0.015$. The stress reaches a maximum of $\bar{\gamma} = 14\,\mathrm{MPa}$ when $\bar{\gamma} = 0.065$. These values are somewhat higher than those reported by Groves *et al.*, for LX-14 in quasi-static tests, which is expected under the high strain rate conditions we study. Failure occurs at $\bar{\gamma} = 0.09$. Observation of the post-test specimen reveals a planar failure with a rough failure surface including small voids. This is as would be expected in microvoid coalescence induced ductile shear fracture.

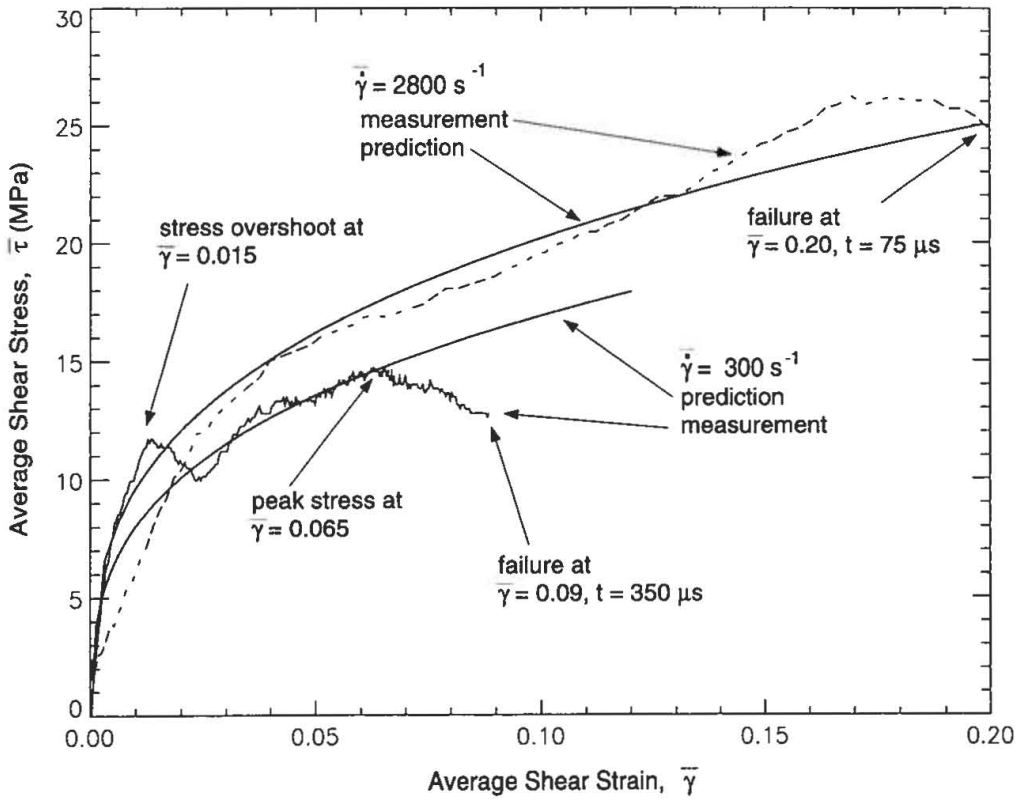

FIGURE 2 Measured average stress *versus* average strain for LX-14 inert simulant (Mock 900–20) along with model predictions at two different strain rates; T_o = 298 K.

The test performed at the higher $\dot{\bar{\gamma}} = 2800\,\mathrm{s}^{-1}$ lasted only 75 μs, due to higher strain rate deformation. No early time overshoot is observed in this test. Failure occurs at $\bar{\gamma} = 0.20$ at which time $\bar{\tau} = 25$ MPa, which is near its peak of 26 MPa. The increase in peak stress as strain rate increases is consistent with the trends observed in the quasi-static tests. Examination of the post-test specimen revealed fragmentation of the center section as well as the flanges. By a fractographic study of fragments, it is determined that cracks initiated in the center section and propagated outward into the flanges at an angle to the axis of the cylinder, which is indicative of brittle failure. The failure mechanism for this material is dependent on loading rate, and in no cases observed is due to shear banding.

It is, however, hypothesized that if observed failure mechanisms were suppressed, such as might occur upon application of hydrostatic stress, localization would occur in the tested materials. Chou *et al.* (1991) stated that brittle reactive materials become more ductile under the application of hydrostatic stresses and concluded that localization becomes significant in mechanically constrained explosives. Also, Dodd and Atkins (1983) report

that increased hydrostatic stresses tend to decrease microvoid nucleation. Deformation under these circumstances could result in the suppression of these other failure mechanisms and hence increase the susceptibility to localization and initiation. Moreover, the heavy confinement which is likely to provide a hospitable environment for shear banding is indeed a likely one for energetic solids to encounter.

4.2. Model Predictions for LX-14

Figure 3 shows the results of a typical reactive shear localization simulation. The velocity profile, Figure 3a, shows a three stage localization process, which was initially observed experimentally in metals by Marchand and Duffy (1988). At the initial state, Stage I, the profile has a linear distribution in space, a state that is often referred to as homogeneous deformation. Since the specimen is thinnest at its center, it is also weakest at that point. Material is thus locally less resistant to deformation in the center, hence an inhomogeneous velocity profile with the greatest slope at the center develops. This is referred to as Stage II. Stage II localization is not readily discerned. As $\dot{\gamma}$ increases, so does τ by Eq. (8) and consequently T by Eq. (16); the combined effect of increased shear stress and shear strain rate causes the temperature to increase. This rise in temperature causes the stress to drop, which results in further straining and further heating. This interaction continues until, after 1.30 ms, thermal softening dominates over strain and strain rate hardening. Consequently, deformation rapidly localizes to a narrow region, referred to as Stage III localization. It is this final stage that is termed shear banding. At this time, the rate of change of temperature increases dramatically at the center of the shear band. The peak strain rate in the shear band, calculated by a finite difference centered over two cells, is predicted to be $5.18 \times 10^4\,\mathrm{s}^{-1}$. This should be considered a lower bound dictated by the finite spatial resolution employed, as it is seen that it is of the same order of magnitude as $(v_1/2\Delta z) = 7 \times 10^4\,\mathrm{s}^{-1}$. The corresponding displacement field is shown in Figure 3b.

Figure 3c shows a plot of the stress field. For $t < 1.30$ ms the stress field rises in a nearly spatially homogeneous manner until it reaches a peak of 50.3 MPa; in this period, strain and strain rate hardening are dominant mechanisms. For $t \geq 1.30$ ms, the stress begins to decrease in a spatially homogeneous manner due to global thermal softening. Thermal softening accelerates at the center of the specimen near the geometrical inhomogeneity, giving rise to a rapid drop of stress, and the consequent localization and reaction.

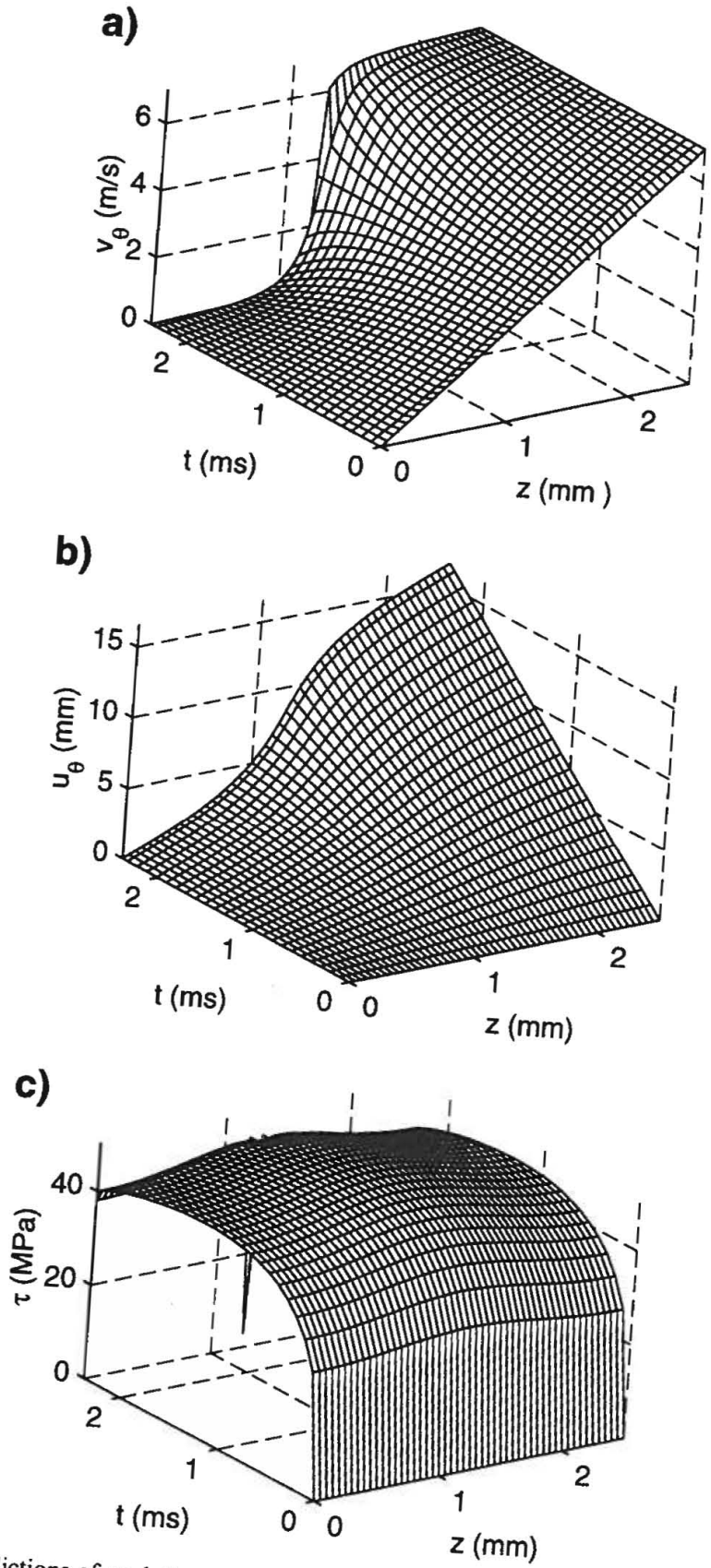

FIGURE 3 Predictions of evolution of (a) velocity v_θ, (b) displacement u_θ, (c) shear stress τ, (d) Zener–Hollomon localization criteria, (e) reaction progress λ and (f) temperature T fields for LX-14 subjected to torsional strain, $\bar{\dot{\gamma}} = 2800\,\mathrm{s}^{-1}$.

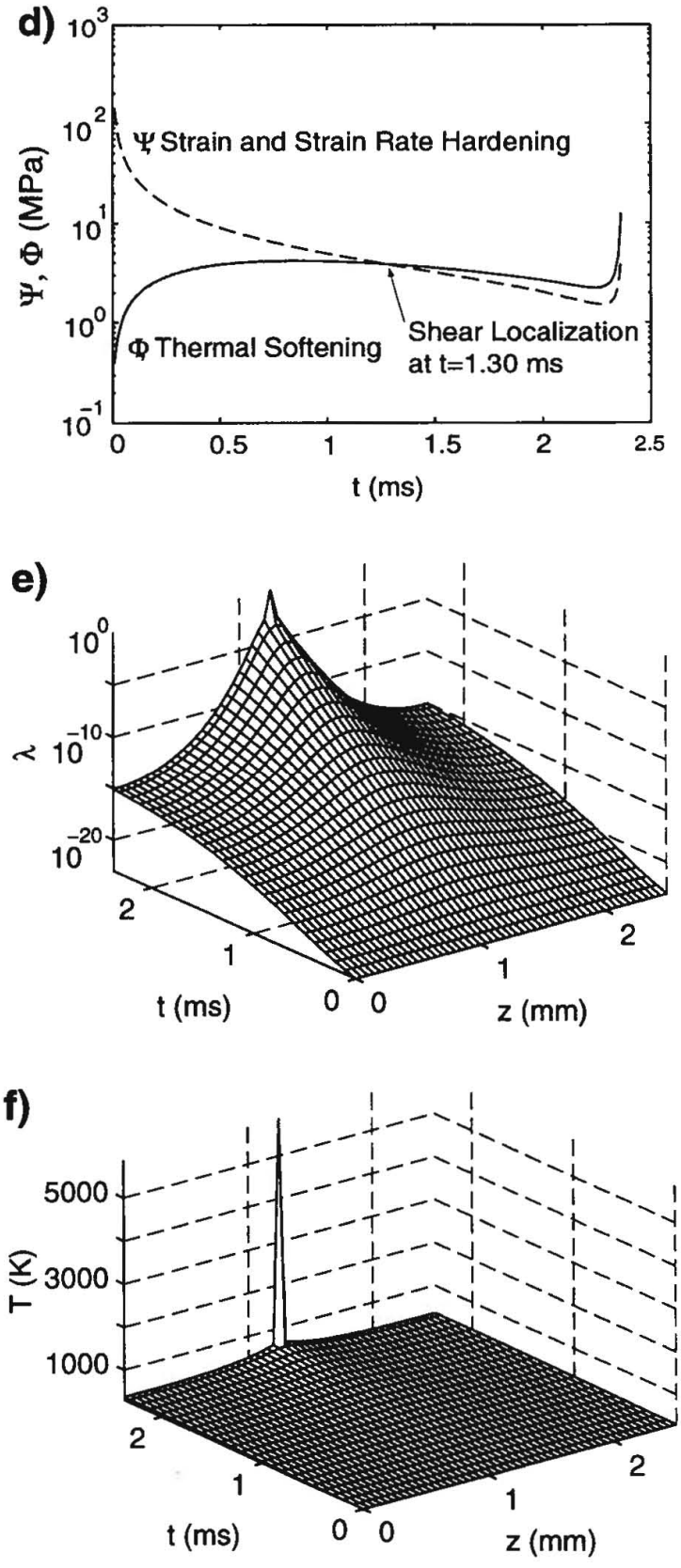

FIGURE 3 (Continued).

Examination of the Zener–Hollomon criterion, Eq. (14) evaluated at the center of the specimen, gives results which are consistent with those of Figure 3c. The right hand side, Φ and left hand side, Ψ, of Eq. (14) are plotted as functions of time in Figure 3d. It is seen that both Φ and Ψ are always positive, indicating that the material is experiencing strain and strain rate hardening as well as thermal softening. The time when $\Psi = \Phi$, $t = 1.30\,\text{ms}$, is necessarily identical to the time of peak stress, and is a good estimate of the onset of localization. Near the end of the calculation, both Ψ and Φ increase sharply. This behavior could in part be a numerical artifact attributable to the previously described coarse spatial resolution in the neighborhood of the shear band; nevertheless, a sharp increase in thermal softening rate is not unexpected upon commencement of rapidly accelerated reaction rate in the reactive shear band.

Significant reaction is predicted shortly following the onset of localization. At this time, reaction initiates in the localized hot spot as seen in Figure 3e, which shows the evolution of λ on a logarithmic scale. Reaction is predicted to proceed extremely quickly, with λ at the center of the specimen increasing from 0.1 to 0.9 in less than 1 ns. Computation is ceased following the complete reaction ($\lambda = 1$) of the center-most cell, as by this time the system of equations is extremely stiff and gives rise to time steps on the order of 10^{-15} s. This is consistent with a simple estimate of reaction time scales, given by $t_R = (1/Z)\exp(E/RT)$, which at a typical reaction zone temperature, $T = 4000\,\text{K}$, yields $t_R = 1.4 \times 10^{-16}\,\text{s}$.

Lastly, shown in Figure 3f are predictions of the temperature field. On the scales of the plot, a relatively small rise in temperature is detectable in the center region of the specimen. Though not obvious on the scale shown in Figure 3f, temperature at the center of the shear band at the onset of localization is 405 K. The shear localization induces reaction which induces an extremely rapid rise in temperature to a value of 5885.1 K in the center most cell at the final time considered. While this value may seem high, it is consistent with a rapid deposition of energy which has had insufficient time to diffuse away. Temperature rise induced by a simple constant volume combustion process in the absence of diffusion is simply $\Delta T = q/c$, which for our baseline case has a value of 5265 K. Given that the material's initial temperature is 298 K and that it experiences additional energy conversion due to plastic work, the temperature predicted is plausible. Furthermore, it is easily verified that on time scales on which the reaction is occurring, diffusion plays an insignificant role in energy transport on the length scales which have been considered. This is verified when one considers the time t_D for a pulse of thermal energy to undergo appreciable diffusion across one

computational cell width, $\Delta z = 50\,\mu m$: $t_D = \rho c \Delta z^2/k$. For the conditions studied, this diffusion time is seen to be 11.9 ms, orders of magnitude greater than the time scales over which this system is evolving during a reactive shear localization, and comparable to the time scale over which the entire event is modelled. In order to render thermal diffusion an important mechanism during a reactive localization event evolving on time scales of 10^{-15} s, consideration of an extremely fine spatial length scale of less than 0.015 nm is required.

4.3. Sensitivity Analysis

A parametric study is performed in order to determine the sensitivity of shear localization to variations in system parameters. In all cases studied, reaction quickly followed localization, so it is fair to view the localization criteria also as an ignition criteria. We perform a series of simulations in which all parameters, save one, are held constant, and examine the effect of variation of the parameter of interest on the time to shear localization, as determined by Eq. (14). Each parameter studied was varied over two orders of magnitude, one below the baseline state, and one above the baseline state, so as to provide a common basis for comparison. It may or may not be possible to induce such changes in actual explosive formulation; nevertheless, this analysis gives intuitive guidelines of relative trends.

Figure 4 gives plots of the time to localization scaled by the baseline time to localization, $t^* = 1.30$ ms, as a function of (a) mechanical and (b) thermochemical parameters scaled by their values at their baseline states (indicated here by a * superscript). It is clear that the localization time (and thus the consequent induction time) is more sensitive to changes in mechanical properties than to most thermochemical properties. The most critical constants are the stress constant α and the imposed velocity v_1, in that an order of magnitude increase in each introduces nearly an order of magnitude reduction in localization time. There is a similar sensitivity to changes in the thermal softening parameter ν; however below a critical value, the localization time becomes relatively insensitive. Localization is hindered by increases in strain rate hardening, and for most of the range studied, strain hardening. The stronger hindrance is due to strain hardening; below a critical value, an order of magnitude of increase induces an order of magnitude increase in localization time. Above a critical value, $\eta/\eta^* \sim 2.5$ ($\eta \sim 0.80$), we predict increases in strain hardening to actually hasten localization. Though the exact reason for this turnabout is unclear, such a result indicates that for this non-linearly coupled system increases in strain

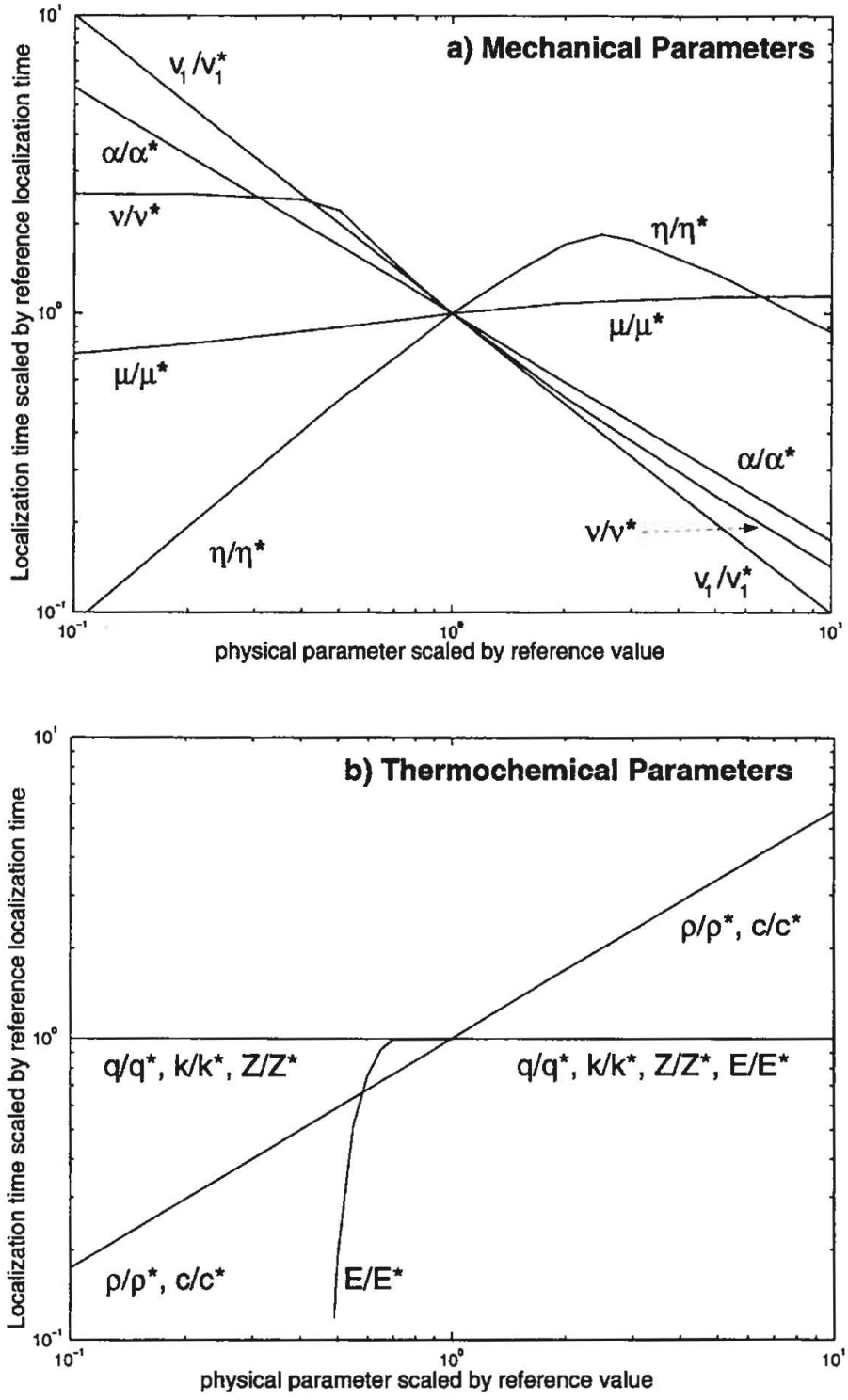

FIGURE 4 Predictions of localization time scaled by baseline case localization time, $t^* = 1.30$ *ms*, as a) mechanical parameters u_1, α, η, μ, ν and b) thermochemical parameters k, c, q, Z, ρ, E, all scaled by their baseline values ($*$), are varied from their baseline states.

hardening can induce changes in temperature as well as stress, and that this dominates for high strain hardening. Increases in strain rate hardening induce a lesser, though still positive, increase in localization time.

On the scales plotted there is essentially no sensitivity of localization time to changes in thermal conductivity, heat release, or kinetic rate constant. On very fine scales, it is seen that localization is hindered by increases in thermal conductivity and hastened by increases in heat release and kinetic rate constant. Though not shown on the plot, an order of magnitude reduction in activation energy reduces the localization time to an unrealistically small value of 7.3×10^{-19} s. Increases in activation energy sharply increase the time to localization, until a critical value, above which the localization time is insensitive to changes in activation energy. Orders of magnitude increases in both density and specific heat induce corresponding orders of magnitude increase in the time to localization.

5. CONCLUSIONS

Predictions of localization and ignition have been given for the first time for a model which allows for time and space dependency, a realistic high strain rate constitutive model, and finite rate exothermic reaction. In all cases studied, ignition was an immediate consequence of a shear localization event. It is also found that localization/ignition is far more sensitive to changes in mechanical properties than to most thermochemical properties. This suggests that explosive designers who are trying to reduce the ignition sensitivity pay special attention to the mechanical properties. While the many limiting assumptions render our results more appropriate for qualitative, rather than quantitative guidance, a framework is present for analyzing systems which model more of the details of real systems. With sufficient details in place, it may be possible to achieve the goal of precise selection of material properties to prescribe an explosive's sensitivity to ignition.

Acknowledgements

R. J. Caspar, J. M. Powers and J. J. Mason are grateful for the support of AFOSR through the Summer Research Extension Program under contracts RDL-96-0871, RDL-96-0870, RDL-96-0847, respectively. The authors also recognize Dr. J. C. Foster, Jr. and Mr. A. Spencer of Wright Laboratory,

Armament Directorate, Eglin AFB, for motivating this study and procuring specimens, respectively and Dr. D. J. Idar and Dr. J. L. Mace of Los Alamos National Laboratory for helpful critical reviews and discussion of the revised manuscript.

References

Baer, M. R. and Nunziato, J. W. (1986) A Two-phase Mixture Theory for the Deflagration to Detonation Transition (DDT) in Reactive Granular Materials. *Int. J. Multiphase Flow*, **12**, 861.

Bai, Y. and Dodd, B. (1992) Adiabatic Shear Localization: Occurrence, Theories, and Applications, Pergammon, New York.

Baker, W. W. and Yew, C. H. (1966) Strain Rate Effects in the Propagation of Torsional Plastic Waves. *J. Appl. Mech.*, **33**, 917.

Boyle, V., Frey, R. and Blake, O. (1989) Combined Pressure Shear Ignition of Explosives. *Ninth Symposium (International) on Detonation*, Office of Naval Research, Arlington, VA, pp. 3–17.

Caspar, R. J. (1996) Experimental and Numerical Study of Shear Localization as an Initiation Mechanism in Energetic Solids. *M. S. Thesis*, University of Notre Dame.

Chen, H. C., Nesterenko, V. F., Lasalvia, J. C. and Meyers, M. A. (1997) Shear-induced Exothermic Chemical-reactions. *J. Physique IV*, **7**, 27.

Chou, P. C., Flis, W. and Jann, D. (1991) Explosive Response to Unplanned Stimuli, Dyna East Corporation Technical Report DE-TR-91-15.

Clifton, R. J., Duffy, J., Hartley, K. A. and Shawki, T. G. (1984) On Critical Conditions for Shear Band Formation at High Strain Rates. *Scripta Met.*, **18**, 443.

Coffey, C. S., Frankel, M. J., Liddiard, T. P. and Jacobs, S. J. (1981) Experimental Investigation of Hot Spots Produced by High Rate Deformation and Shocks. *Seventh Symposium (International) on Detonation*, Naval Surface Weapons Center, Annapolis, MD, pp. 970–975.

Coffey, C. S. (1989) Initiation of Explosive Crystals by Shock or Impact. *Ninth Symposium (International) on Detonation*, Office of Naval Research, Arlington, VA, pp. 58–65.

Dienes, J. K. (1986) On Reactive Shear Bands. *Phys. Letters A*, **118**, 433.

Dilellio, J. A. and Olmstead, W. E. (1997) Shear-band Formation Due to a Thermal Flux Inhomogeneity. *SIAM J. Appl. Math.*, **57**, 959.

Dobratz, B. M. and Crawford, P. C. (1985) LLNL Explosives Handbook–Properties of Chemical Explosives and Explosive Simulants, Lawrence Livermore National Labs., UCRL-52997, National Technical Information Service, DE91-006884.

Dodd, B. and Atkins, A. G. (1983) Flow Localization in Shear Deformation of Void-containing and Void-free Solids. *Acta Metall.*, **31**, 9.

Eiland, P. F. and Pepinsky, R. (1955) The Crystal Structure of Cyclotetramethylene Tetranitramine, *Zeitschrift für Kristallographie*, **106**, 18.

Fickett, W. and Davis, W. C. (1979) Detonation, University of California Press, Berkeley.

Field, J. E., Swallowe, G. M. and Heavens, S. N. (1982) Ignition Mechanisms of Explosives During Mechanical Deformation, *Proc. R. Soc. London A*, **382**, 231.

Field, J. E., Palmer, S. J. P., Pope, P. H., Sundararajan, R. and Swallowe, G. M. (1985) Mechanical Properties of PBX's and their Behaviour During Drop Weight Impact. *Eighth Symposium (International) on Detonation*, Naval Surface Weapons Center, Annapolis, MD, pp. 635–644.

Frey, R. B. (1981) The Initiation of Explosive Charges by Rapid Shear. *Seventh Symposium (International) on Detonation*, Naval Surface Weapons Center, Annapolis, MD, pp. 36–42.

Groves, S., DeTeresa, S., Logan, R., Sanchez, R., Andreski, H., Cunningham, B. and Chiu, I. (1998) Accelerated Aging and Mechanical Modeling of Plastic Bonded Explosives, Lawrence Livermore National Laboratory, UCRL-ID-129483.

Gray, G. T., Blumenthal, W. R., Idar, D. J. and Cady, C. M. (1997) Influence of Temperature on the High-strain-rate Mechanical Behavior of PBX 9501, Los Alamos National Laboratory, LA-UR-97-2894.

Hartley, K. A., Duffy, J. and Hawley, R. H. (1985) The Torsional Kolsky (Split-Hopkinson) Bar, High Strain Rate Shear Testing in High Strain Rate Testing, Mechanical Testing, Metal Hand Book, American Society for Metals, Vol. 8, Edition 9, pp. 218–230.

Hindmarsh, A. C. (1983) ODEPACK, A Systematized Collection of ODE Solvers, Scientific Computing, Stepleman, R. S. *et al.*, Ed., IMACS/North-Holland Publishing Company, Amsterdam, pp. 55–64.

Howe, P. M., Gibbons, G. and Webber, P. (1985) An Experimental Investigation of the Role of Shear in Initiation of Detonation by Impact. *Eighth Symposium (International) on Detonation*, Naval Surface Weapons Center, Annapolis, MD, pp. 294–301.

Johnson, G. R. and Cook, W. H. (1983) A Constitutive Model and Data for Metals Subjected to Large Strains, High Strain Rates and High Temperatures. *Proc. 7th Int. Symp. Ballistics*, The Hague, The Netherlands, pp. 541–548.

Kipp, M. E. (1985) Modeling Granular Explosive Detonations with Shear Band Concepts. *Eighth Symposium (International) on Detonation*, Naval Surface Weapons Center, Annapolis, MD, pp. 35–41.

Marchand, A. and Duffy, J. (1988) An Experimental Study of the Formation Process of Adiabatic Shear Bands in a Structural Steel. *J. Mech. Phys. Sol.*, **36**, 251.

Mohan, V. K., Bhasu, V. C. J. and Field, J. E. (1989) Role of Adiabatic Shear Bands in Initiation of Explosives by Drop-weight Impact, *Ninth Symposium (International) on Detonation*, Office of Naval Research, Arlington, VA, pp. 1276–1283.

Swallowe, G. M. and Field, J. E. (1981) Effect of Polymers on the Drop- Weight Sensitiveness of Explosives, *Seventh Symposium (International) on Detonation*, Naval Surface Weapons Center, Annapolis, MD, pp. 24–35.

Whitham, G. B. (1974) Linear and Nonlinear Waves, John Wiley, New York.

Wiegand, D. A. (1996) Constant Critical Strain for Mechanical Failure of Several Particular Polymer Composites and Other Materials, *Proceedings of the Army Science Conference*, Norfolk, Virginia.

Zener, C. and Hollomon, J. F. (1944) Effect of Strain Rate upon Plastic Flow of Steel, *J. Appl. Phys.*, **15**, 22.